scientific reports

Check for updates

OPEN

Integrated analysis and experimental validation reveal the prognostic and immunological features associated with coagulation in hepatocellular carcinoma

Guangzhen Qu[1], Kun Liu[2], Weiyu Xu[2] & Dongming Li[3]✉

Coagulation is intensively related to various tumors, which affects their progression and prognosis. However, research on the impact of coagulation-associated genes (CAGs) on hepatocellular carcinoma (HCC) occurrence, prognosis, and immune microenvironment is limited. Consequently, our research aims to uncover how CAGs affect the prognosis and immune microenvironments of HCC. We integrated gene expression data and clinical information from three datasets (GSE14520, GSE76427, and TCGA-LIHC). 281 CAGs were obtained from the coagulation-related pathway (hsa04610). We obtained three CAG patterns through a consensus clustering algorithm. Afterward, differential analyses of prognosis, biological processes, immune infiltration, and functional and pathway enrichment were conducted on the three CAG patterns. We intersected CAGs with differentially expressed genes in GSE76427 and then conducted Cox regression analysis to obtain the prognostic genes in HCC. Glycerol-3-phosphate dehydrogenase 2 (GPD2) was selected for further analyses. TCGA-LIHC samples with different GPD2 expression levels were analyzed for prognosis, DNA methylation, immune infiltration, and drug sensitivity. The expression level of GPD2 was verified through quantitative real-time PCR (qPCR) and immunohistochemistry. The wound-healing and Transwell assays were used to analyze the tumor cell migration and the Matrigel invasion and apoptosis assays were performed to determine cell invasion and apoptosis. Three CAG patterns were obtained through an unsupervised consensus clustering algorithm. CAGclusterA held the best prognosis compared to the other two clusters. The CAGclusterC was characterized by poor prognosis and abundant immune cell infiltration. The TCGA-LIHC dataset, as an internal validation, also yielded similar subtype classifications. Afterward, we identified the GPD2 gene, which significantly affected the prognosis of HCC and was positively correlated with the tumor progression. The upregulation of GPD2 expression was closely related to tumorigenic signatures and immune escape. The qPCR confirmed the upregulation of GPD2 expression in HCC tumor cell lines, compared to normal liver cell lines. Immunohistochemical staining confirmed the high expression of GPD2 in HCC tumor tissues compared to normal tissues. Regulating the expression level of GPD2 can inhibit the proliferation, migration, invasion, and induce apoptosis of HCC cells. Our study comprehensively elucidated the coagulation characteristics in HCC and identified a promising oncogenic gene GPD2. Exploring targeted strategies based on coagulation-related characteristics and biomarkers may shed light on HCC treatment.

Keywords Coagulation-associated genes, Consensus clustering algorithm, Immune infiltration, Hepatocellular carcinoma, GPD2

[1]Department of Interventional Radiology, Beijing Chao-Yang Hospital Affiliated with Capital Medical University, Beijing 100020, China. [2]Department of General Surgery, Beijing Friendship Hospital, Capital Medical University, Beijing 100050, China. [3]Department of Gastric and Colorectal Surgery, General Surgery Center, The First Hospital of Jilin University, Changchun 130021, China. ✉email: doctorlee2020@163.com

Hepatocellular carcinoma (HCC) is the fifth most common malignant tumor in the world, accounting for the third leading cause of cancer death, with China accounting for more than half of new cases and deaths[1]. A variety of traditional treatments are used to treat HCC, such as surgery, chemotherapy, radiation therapy, and interventional therapy[2]. In recent years, molecularly targeted drugs represented by sorafenib and immune checkpoint inhibitors have successfully improved the treatment status of advanced HCC patients to a certain extent. Furthermore, the recent success of atezolizumab (anti-PD-L1) combined with bevacizumab (anti-VEGF) marks an important change in the first-line treatment of advanced HCC[3]. However, the inherent limitations of traditional approaches make effective treatment of HCC unsatisfactory[4].

The coagulation system is closely related to tumor innate defense mechanisms and tumor microenvironment (TME). Experimental data have shown that patients with malignant tumors often tend to have chronic hypercoagulability and high fibrillation[5]. Complications of venous thromboembolism are usually potential symptoms of malignant tumors. Portal vein thrombosis is the most common type of coagulation-related symptoms in patients with HCC[6]. Coagulation may be the joint effect of bleeding and intravascular coagulation caused by vascular wall rupture, or it may be caused by the activation of extravascular coagulation due to increased vascular permeability and plasma extravasation[7]. Fibrin in the coagulation system is initially a temporary matrix. It provides a favorable substrate for the attachment and migration of tumor cells[7]. Meanwhile, coagulation system disorders are associated with tumor progression and prognosis[8]. The liver can synthesize coagulation factors, but in some liver diseases, such as liver cirrhosis, autoimmune liver disease, and HCC, the coagulation system is often dysfunctional. Research has shown that tissue factors from exogenous coagulation pathways can promote the occurrence of HCC[9]. In patients with HCC, Von Willebrand factor antigen can be used as a marker of prognosis, which correlates closely with postoperative complications and long-term outcomes[10]. Protein Induced by Vitamin K Absence II is considered a novel circulating marker in HCC and has a certain value in the diagnosis of early HCC[11,12]. Yin et al.'s study suggested a correlation between coagulation-associated genes and immunotherapy and the prognosis of clear cell renal cell carcinoma[13]. Wang et al.[14] constructed a survival and prognosis model for gastric cancer based on coagulation-associated genes, which has high accuracy. Studies have shown that the abnormal expression of urokinase-type plasminogen activator and plasmin activator fibrinolysis system inhibitor-1 is also a risk factor for the prognosis, recurrence, and metastasis of breast cancer[15]. As a result, the complex coagulation system can affect the occurrence, proliferation, and prognosis of several tumors. The tumor coagulation process is a molecular effector network that promotes thrombosis and bleeding in cancer cells and has been the hotspot of tumor research. Cancer treatment plans based on coagulation-related genes may open up new avenues.

In our study, the unsupervised consensus clustering algorithm was performed to identify coagulation-associated genes (CAGs) patterns from The Cancer Genome Atlas (TCGA) and Gene Expression Omnibus (GEO) datasets. A comparison was performed on immune cell infiltration, immune-related pathways, survival curves, and biological processes among three HCC patterns. Differential expression gene analysis was conducted between HCC tumor samples and normal samples in the GSE76427 dataset, and 50 common genes were obtained by intersecting with CAGs. Cox regression analysis identified four genes associated with HCC prognosis and Glycerol-3-phosphate dehydrogenase 2 (GPD2) was screened for further analyses. Upregulation of GPD2 expression is significantly associated with poor overall survival, higher tumor grade, and $CD4^+$ Th2 cell immune infiltration in HCC. Multiple HCC datasets confirm that GPD2 is significantly upregulated in HCC tumor tissues compared to normal tissues. Furthermore, we conducted quantitative real-time PCR (qPCR) experiments to verify the expression difference of GPD2 in HCC cell lines and normal liver cells. We used paraffin sections of HCC tumor tissue and adjacent tissues for immunohistochemical analysis to compare the expression extension of GPD2. The cell proliferation assay, wound-healing assay, Transwell assay, Matrigel invasion assays, and apoptosis assays were performed to observe the regulator roles of GPD2 in proliferation, migration, invasion, and apoptosis after GPD2 inhibition by small interfering RNA (siRNA).

Methods

Data collection and preprocessing

Gene expression profiles and corresponding clinical datasets for hepatocellular carcinoma were obtained from GSE14520 ($n=246$) and GSE76427 ($n=115$) datasets of GEO database (https://www.ncbi.nlm.nih.gov/geo/) and TCGA-liver hepatocellular carcinoma (LIHC) dataset ($n=377$) of TCGA database (https://gdc.cancer.gov/). The samples with incomplete information or duplicates were excluded. Finally, a total of 728 HCC samples were collected and integrated into a meta-LIHC cohort. The raw data in the microarray dataset obtained from GEO were proceeded and normalized using a robust multichip average (RMA) algorithm implemented in the "affy (v1.84.0)" R package[16]. The data format of TCGA-LIHC dataset was transformed from the fragments per kilobase of script per million mapped reads (FPKM) to the transcripts per million (TPM). The meta-LIHC datasets with the batch effect removed were used as the training set, while TCGA-LIHC was used as the internal validation set. The hsa04610 (complement and coagulation cascade) including 281genes was obtained from the Kyoto Encyclopedia of Genes and Genomes (KEGG) database (https://www.genome.jp/kegg/) as a coagulatio n-associated gene set. A total of 255 CAGs (Supplementary Table S1) intersected in the TGCA-LIHC, GSE14520, and GSE76427 datasets were ultimately obtained for further analyses.

Unsupervised consensus clustering analysis

Based on the CAGs obtained from hsa04610, unsupervised consensus clustering analysis was performed in the meta-LIHC dataset using the "ConsensusClusterPlus (v1.70.0)" R package to determine the number of clusters and classify patients into distinct coagulation-associated gene clusters (CAGclusters). In the TCGA-LIHC dataset for internal validation, we performed the same unsupervised clustering algorithm based on the CAGs and also divided samples into different patterns. To ensure the stability of consensus classification, we

executed and repeated this program 1000 times. In addition, we conducted differential expression analysis on CAGclusters and plotted visual heatmaps. We conducted a Kaplan-Meier analysis of the overall survival (OS) between the different CAGclusters using the "survival (v3.3.1)" R package.

Immune cell infiltration in tumor microenvironment in CAG patterns

The immune system is composed of specific immunity (adaptive immunity) and non-specific immunity (innate immunity). The innate immune system is our first line of defense, but it is non-specific. Its roles are to recognize foreign pathogens and trigger inflammation, engulf foreign molecules and cells, or present them to the adaptive immune system[17]. By establishing antigen-specific reactions to destroy pathogens, adaptive immunity allows the body to recognize the distinctive antigens of pathogens[18]. The immune cell infiltration in the TME plays an indelible role in the occurrence, progress, and metastasis of tumors. The single sample gene set enrichment analysis (ssGSEA) was conducted via the "GSVA (v1.44.5)" R package to identify the characteristics of immune cell infiltration in the tumor immune microenvironment between different CAGclusters. The immune infiltration of innate immune cells (such as dendritic cells, eosinophils, mast cells, macrophages, natural killer cells, and neutrophils) and adaptive immune cells (such as B cells, T cells, T helper cells, $CD8^+$ T cells, regulatory T cells, and cytotoxic cells) in TME of different CAGclusters was explored. The heatmap of immune cell infiltration in different samples of CAGclusters was visualized.

Biological process and functional analysis in CAG patterns

In different CAGclusters, we used the ssGSEA to identify the differences in biological processes and pathway enrichment. The Gene Ontology (GO) enrichment analysis based on CAGs was also performed and the top 10 GO enrichment terms were selected for visualization. The enrichment scores of multiple biological processes, such as angiogenesis signature, stromal-activation-relevant signatures, mismatch repair-relevant signatures, antigen processing, and immune activation-relevant signatures, were also analyzed in different CAG patterns. In addition, we demonstrated the expression differences of specific genes such as major histocompatibility complex (MHC), costimulatory, and adhesion molecules in different CAGclusters.

Identification of differential expression genes (DEGs) and prognostic analysis

The GSE76427 includes information on 115 HCC samples and 52 normal liver tissue samples, which were used to perform DEG analysis. With the cutoff values set to log2 fold change (FC) > 1 and adjusted $P < 0.01$, the upregulated DEGs were obtained through the "limma (v3.52.2)" R package. Subsequently, the upregulated DEGs in GSE76427 were intersected with CAGs. The obtained intersection genes were used for univariate Cox analysis in HCC and prognostic genes were identified. The Kaplan-Meier curves of the selected target gene were plotted. In addition, we compared the expression differences of selected target gene between tumor tissue and normal tissue in multiple HCC datasets (GSE14520, GSE76427, GSE45114, GSE54236, GSE64041, and GSE17856) of the GEO database.

Roles of GPD2 in the immune microenvironment and biological process

For the selected GPD2 gene, we analyzed its relationship with immune cell infiltration in TCGA-LIHC and several vital immune-gene features, such as T cell-inflamed gene expression profile (GEP), cancer-associated fibroblasts (CAF), tumor-associated macrophages (TAM) M2, interferon-gamma (IFNG), CD8, CD274, tertiary lymphoid structure (TLS), T cell dysfunction, T cell exclusion, and myeloid-derived suppressor cells (MDSC). Meanwhile, the relationship between the GPD2 gene and immune checkpoints and the immunological markers related to T cell activation, neutrophil activation, and regulation of inflammatory response were analyzed. The Tracking Tumor Immunophenotype (TIP) database (http://biocc.hrbmu.edu.cn/TIP/) was also used to analyze the impact of GPD2 on the cancer immunity cycle of HCC. Based on the ssGSEA algorithm, we sequentially calculated the enrichment scores of each TCGA-LIHC sample on the tumor-related signal pathway and then analyzed the correlation between the GPD2 expression and these pathways. In addition, we visualized the GPD2 DNA methylation and the relationship between GPD2 expression and clinical data using the MEXPRESS database (https://mexpress.be/). Moreover, we explored the differences in anti-tumor drug sensitivity between different GPD2 expression levels in TCGA-LIHC samples via the "pRRophetic (v0.5)" R package.

Cell culture and siRNA transfection

Liver tumor cell lines HepG2 and Huh7 were obtained from Fenghui Biotechnology (Hunan, China) and cultured in DMEM supplemented with 10% fetal bovine serum (FBS) and 5% CO_2 at 37 ℃. Normal liver cell line LO2 cells cultured in RPMI1640 containing 20% FBS. GPD2 siRNA was purchased from Likeli Biotechnology (Beijing, China) and transfected into cells using Lipofectamine 2000 (Invitrogen, CA, USA) according to the manufacturer's instructions. The sequence of siGPD2-1: sense 5′- GCAGUUAUGUCCUCAGCAATT-3′ and antisense 5′-UUGCUGAGGACAUAACUGCTT-3′; The sequence of siGPD2-2: sense 5′- CCUGAGUUGUGA UGUUGAATT-3′ and antisense 5′- UUCAACAUCACAACUCAGGTT-3′.

Quantitative real-time PCR

To determine the expression level of the target gene, we extract total mRNA using the RNApure Tissue Cell Kit (DNase I) (CWBIO, Jiangsu, China) based on the manufacturer's instructions. Reverse transcription was conducted via the HiFiScript gDNA Removal RT MasterMix (CWBIO, Jiangsu, China) according to the manufacturer's instructions. The qPCR was performed using the MagicSYBR Mixture (CWBIO, Jiangsu, China). GAPDH was used as an internal reference gene for detection. The primer sequences are as follows: GAPDH forward, 5′-GCACCGTCAAGGGCTGAAC-3′; GAPDH reverse, 5′-ATGGTGTGAGAGAGAGCAGT-3′;

GPD2 forward, 5′-GAGCTTGGGCTTGGTCTTCC-3′; GPD2 reverse, 5′-TCCCTAGGCCTACAGACGTG-3′. The $2^{-\Delta\Delta Ct}$ was used to analyze the relative mRNA expression level of the GPD2 gene.

Immunohistochemistry (IHC) staining

The IHC staining was performed on tissue paraffin sections similar to that described in previous study[19]. The recombinant anti-GPD2 antibody (ab182144, Abcam, Shanghai, China) was utilized for IHC. The tissues were incubated with indicated antibodies and positively stained cells were then visualized using the DAB Detection Kit (Gene Tech, Shanghai, China) according to the manufacturer's instructions. Following counterstaining with hematoxylin, images were captured under a microscope.

CCK-8 assay

Selected HCC cells with appropriate cell density and inoculated them into DMEM medium containing 10% FBS in 96-well plates (10, 000 cells/well) after transfection with siRNA. The cell viability was detected at 24 h, 48 h, and 72 h after siRNA transfection. The CCK-8 (UE, Shanghai, China) was added and the absorbance at 450 nm was measured using a microplate reader.

Colony formation assay

The transfected cells were inoculated into 6-well plates (1, 000 cells/well), cultured in incubators for 7 days, fixed with 4% paraformaldehyde, washed with PBS, and then stained with 0.1% crystal violet for 5 min. The number of colonies was determined via ImageJ software (v1.4.3.67).

Wound-healing assay

HCC cells were seeded into 6-well plates (1×10^6 cells/well). When the cells grow to a density of 90-100%, the scratches were made on the monolayer cells using the tip of a sterile pipette to create a uniform gap. Rinsed cells with PBS until no floating cells were present and added the FBS-free medium. The scratch data was recorded under a microscope at 0 and 48 h. ImageJ software was used to measure the distance of cell migration.

Transwell migration and invasion assays

HCC cells were resuspended in the serum-free medium, and 1×10^5 cells were seeded into the upper chamber. The 600 µL medium containing 10% FBS was added to the lower chamber. After the cells were incubated for 24 h, the non-migrating cells were wiped off from the upper chamber using cotton swabs, and the migrating cells were fixed with 4% paraformaldehyde and stained with 0.1% crystal violet. Calculated the number of migrating cells from at least five random microscopic fields per membrane. Besides, the membrane surface of the Transwell chambers was coated with 100 µL Matrigel diluted at a 1:8 ratio and incubated for 3 h. The transfected HCC cells in the FBS-free medium were inoculated into the upper chamber. The following operation steps are consistent with the Transwell migration assay.

Apoptosis assay

HCC cells were seeded on 6-well plates with 2×10^5 cells per well and cultured for 24 h. The cells were transfected with siRNA and then cultured for 48 h. YF®488- Annexin V and PI Apoptosis Kits (UE, Shanghai, China) were used to evaluate cell apoptosis. The apoptotic cells were detected by flow cytometry.

Statistical analyses

Bioinformatics analysis was conducted using R software (v4.1.2) downloaded from R Project (https://cran.r-project.org/) on February 28, 2022. The data is expressed as mean ± standard deviation. Univariate Cox regression analysis was used to evaluate the impact of intersected genes on the OS of TCGA-LIHC. The normal distribution data were compared between two groups using the unpaired Student's t-test, while the non-normal distribution data were compared using the Mann-Whitney test. One-way ANOVA was used to evaluate the difference of multiple groups. The P-value < 0.05 was considered statistically significant. The study was approved by the Ethics Committee of Beijing Friendship Hospital (No. 2023-P2-145-01).

Results

Identification of CAG patterns

The flow chart of this study is unveiled in Fig. 1. We merged two GEO datasets (GSE14520 and GSE76427) and one TCGA dataset (TCGA-LIHC) of HCC into the meat-LIHC dataset. Based on 255 CAGs shared in the GEO and TCGA datasets, different CAGclusters patterns were obtained by unsupervised consensus clustering analysis. The k = 3 was considered as the optimal number of clusters, and clusters were defined as CAGclusterA (n = 178), CAGclusterB (n = 340), and CAGclusterC (n = 183), respectively (Fig. 2A). The differential expression of CAGs between different CAGclusters was shown in Fig. 2B. The Kaplan-Meier survival curves showed statistically significant differences in OS among the three patterns, with CAGclusterA having the best prognosis, followed by CAGclusterB and CAGclusterC (Fig. 2C).

Immune infiltration and biological process of CAG patterns in meta-LIHC

The ssGSEA was used to calculate immune cell infiltration in different CAGclusters. The immune infiltration characteristics of CAGclusterA were Th17 cells and eosinophils. The CAGclusterC was characterized by natural killer T cells, plasmacytoid dendritic cells, central memory $CD4^+$ T cells, natural killer cells, activated $CD4^+$ T lymphocytes, activated dendritic cells, memory $CD8^+$ T cells, T follicular helper (Tfh) cells, macrophages, regulatory T cells (Tregs), and MDSC. In CAGclusterB, the main immune infiltrating cells were monocytes, neutrophils, and central memory $CD8^+$ T cells (Fig. 3A). Afterward, we conducted the KEGG pathway analysis

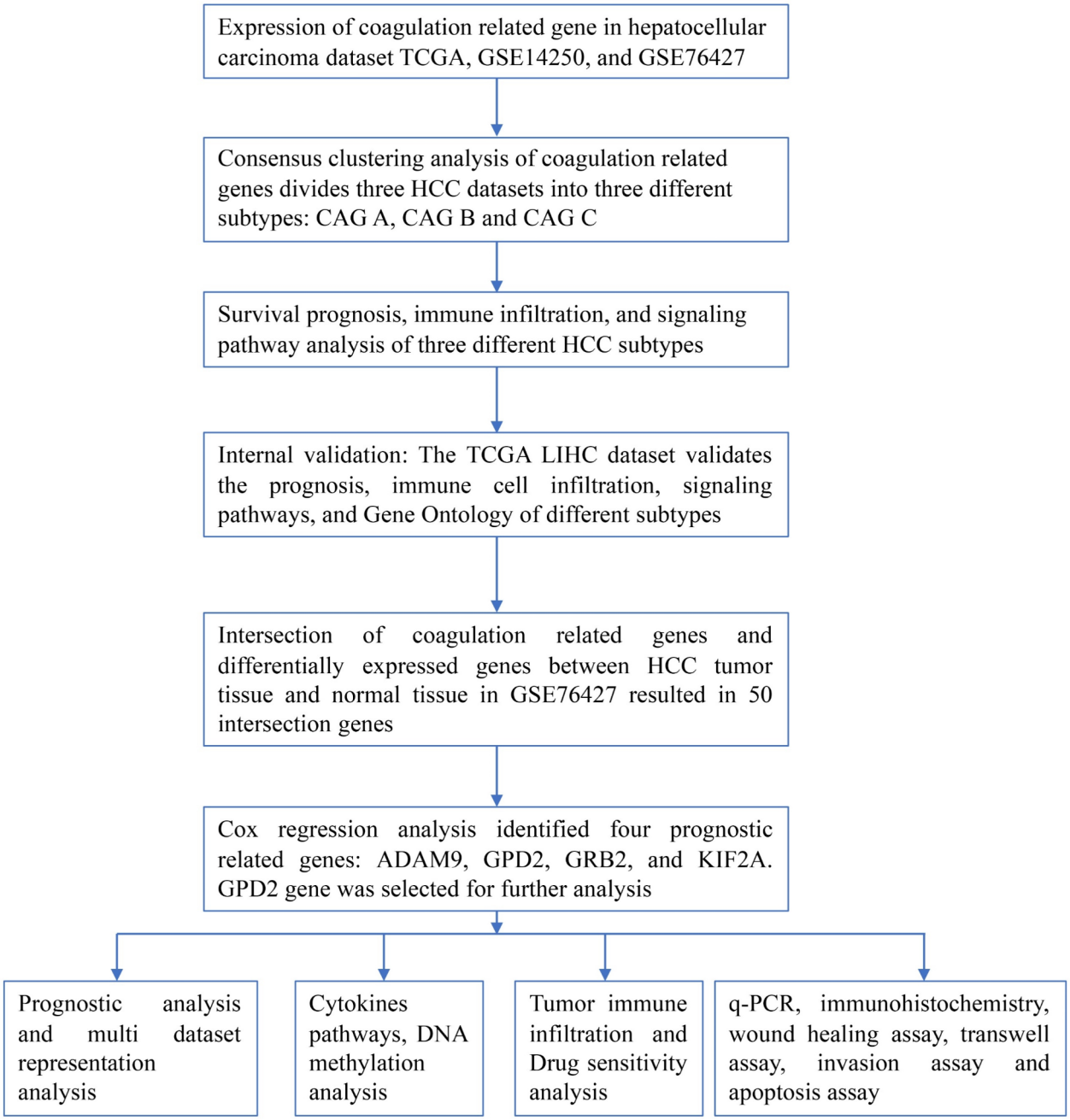

Fig. 1. The flowchart of our study.

on CAG patterns. The relevant activated pathways in CAGclusterA were the WNT signaling pathway, ubiquitin regulatory pathway, and neuroactive ligand-receptor interaction pathway. CAGclusterB was closely related to metabolism-related pathways, such as complement and coagulation metabolism cascades, drug metabolism cytochrome P450, and fatty acid metabolism. CAGclusterC was significantly activated in carcinogenic pathways, such as the transforming growth factor (TGF)-β signaling pathway, WNT signaling pathway, NOTCH signaling pathway, mTOR signaling pathway, MAPK signaling pathway, and JAK-STAT signaling pathway (Fig. 3B). This could explain the fact that in CAGclusterC, tumor-related pathways are active, leading to abundant immune cell infiltration, and its OS is worse than that of CAGclusterA and CAGclusterB. The ssGSEA analysis of specific gene sets has demonstrated a strong correlation between CAGclusterC and epithelial-mesenchymal transition (EMT), WNT signaling pathway, pan-fibroblast TGF-β response signature (Pan-F-TBRS), antigen processing machinery, $CD8^+$ T effector, cell cycle, cell cycle regulators, and DNA damage repair (Fig. 3C). The MHC molecules, costimulatory molecules, and adhesion molecules were significantly differentially expressed in different CAG patterns, and almost all of them were upregulated in CAGclusterC (Fig. 3D).

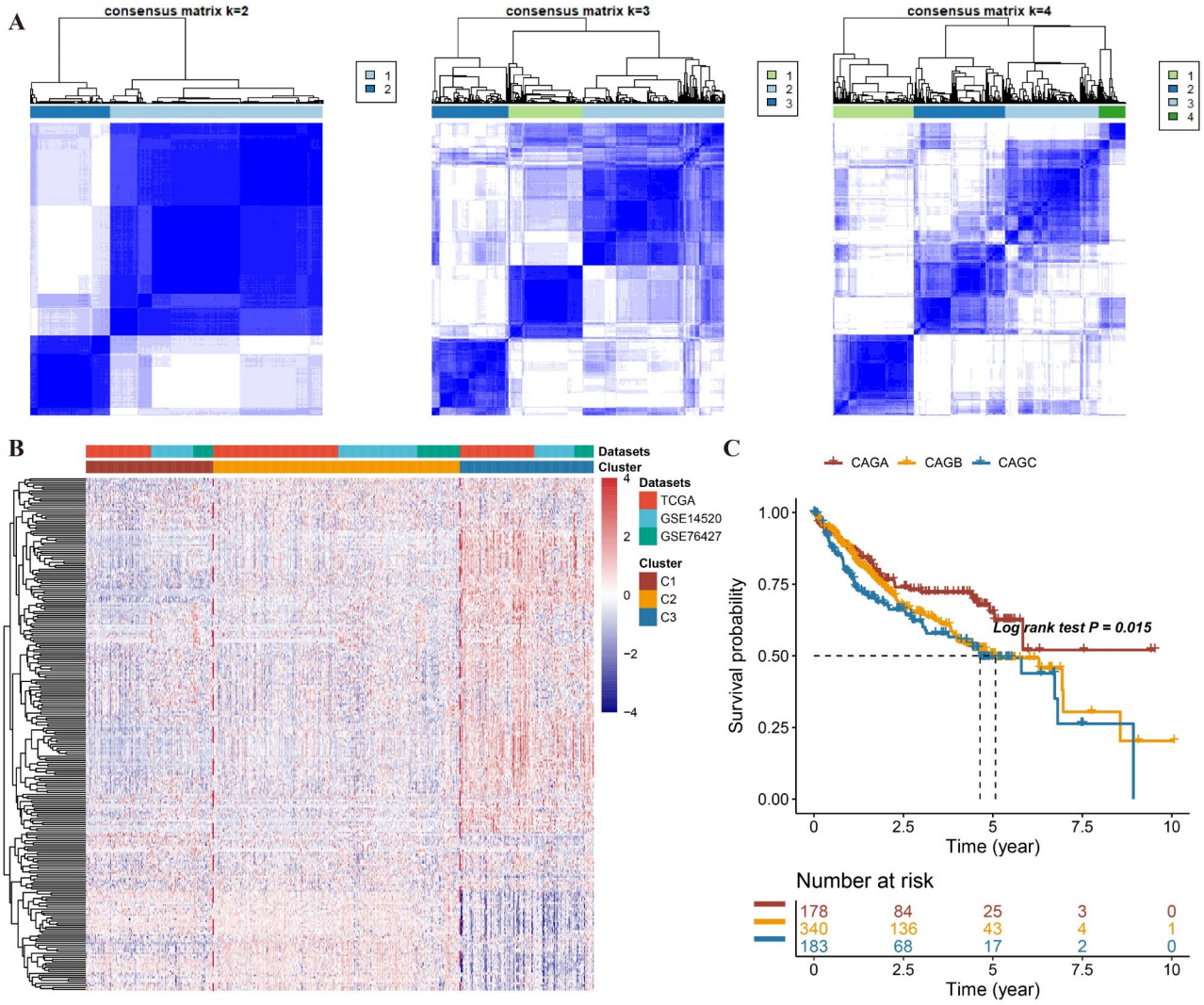

Fig. 2. Consensus cluster analysis based on coagulation-related genes in hepatocellular carcinoma. (A) Consensus cluster analysis was performed in the meta-LIHC cohort (GSE14520, GSE76427, and TCGA-LIHC) for k = 2–4. (B) Hierarchical clustering of coagulation-related genes in the meta-LIHC cohort. (C) Kaplan-Meier curves with a log-rank test of different coagulation-related patterns in the meta-LIHC cohort.

Immune infiltration and biological process of CAG patterns in TCGA-LIHC

We also performed unsupervised clustering algorithms on the TCGA-LIHC dataset based on CAGs and obtained three CAGclusters similar to meta-LIHC. The Kaplan-Meier curves of OS in the three CAG patterns indicated that although the difference was not significant, similar to meta-LIHC, CAGclusterA had the best OS, followed by CAGclusterB and CAGclusterC (Fig. 4A). The expression of MHC molecules, costimulatory molecules, and adhesion molecules were most significant in CAGclusterC, followed by CAGclusterB and CAGclusterA (Fig. 4B), similar to the results in meta-LIHC. The distribution of primary immune cell enrichment fractions in different CAGclusters is shown in Fig. 4C. The GO enrichment analysis was executed based on the DEGs of each cluster (Supplementary Table S2). The main enrichment terms in CAGclusterA were antigen binding, immunoglobulin receptor binding, signaling receptor activator, and receptor-ligand pathway. The terms enriched in CAGclusterB were the least, mainly including passive transmembrane transporter and channel activity pathways. The enrichment terms of CAGclusterC were similar to that of CAGclusterA (Fig. 4D). The CAG patterns in TCGA-LIHC were similar to those in meta-LIHC in terms of OS, signaling pathways, and immune infiltration, which further proves the reliability of HCC clustering based on CAGs.

Target gene screening based on DEGS and prognostic analysis

We conducted DEG analysis between tumor and para-cancer tissues using the GSE76427 dataset, with log2 FC > 1 and adjusted $P < 0.01$. After that, we obtained 6451 upregulated genes and 2207 downregulated genes (Fig. 5A). The intersection of upregulated DEGs and CAGs yielded 50 shared genes (Fig. 5B) (Supplementary Table S3). Univariate Cox analysis of intersection genes in HCC identified 4 genes associated with poor prognosis

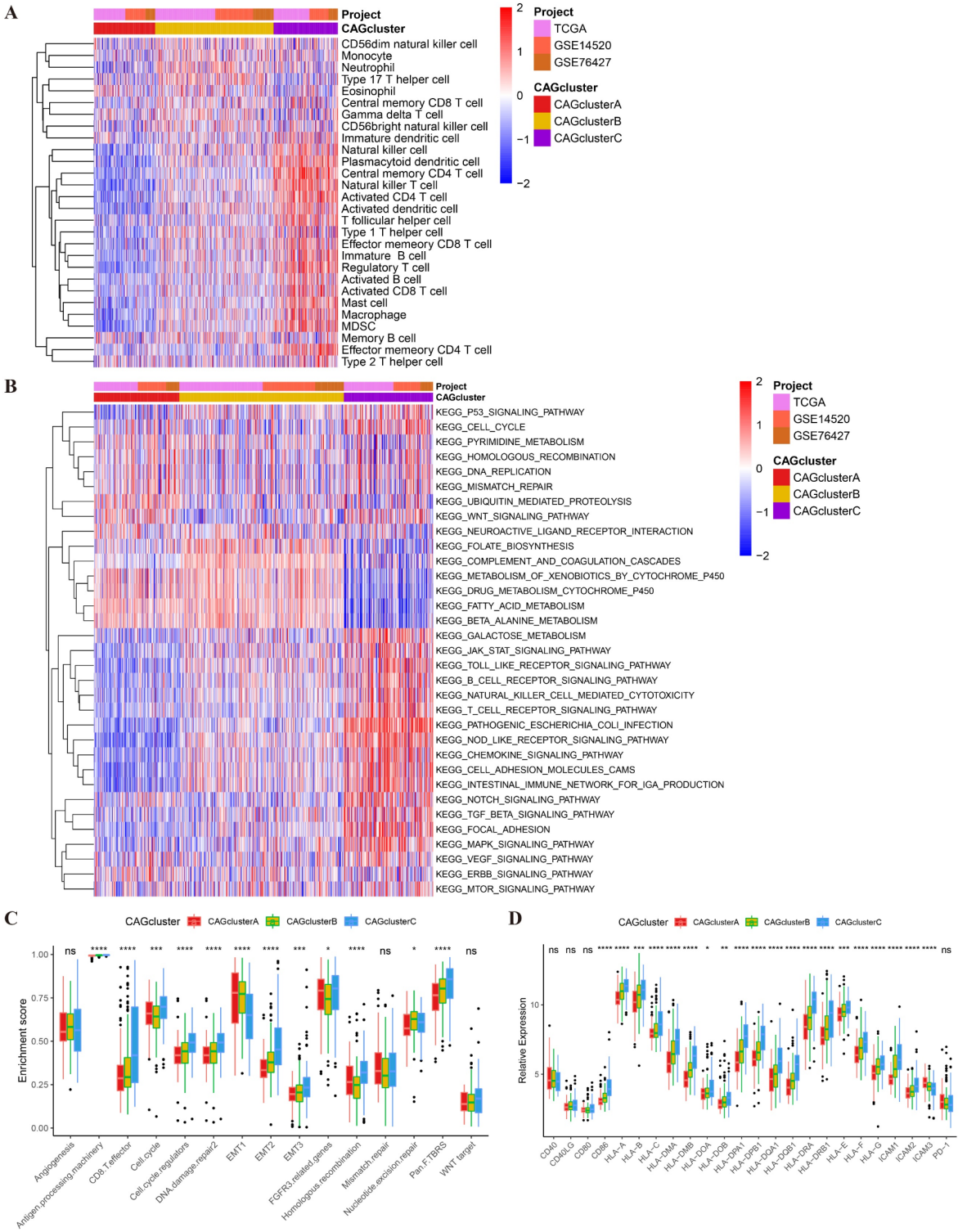

Fig. 3. Characteristics of immune cell infiltration and signal pathway in different coagulation-related patterns in the meta-LIHC cohort. (A) Hierarchical clustering analysis of immune cell infiltration in HCC patients. (B) The single-sample gene sets enrichment analysis showed the discrepancy of biological signaling pathways between different coagulation-related patterns. (C) Discrepancy of stromal-activation-relevant signatures, mismatch repair-relevant signatures, and immune activation-relevant signatures in three coagulation-related patterns. (D) Differential expression of costimulatory molecules, MHC molecules, and adhesion molecules in three coagulation-related patterns.

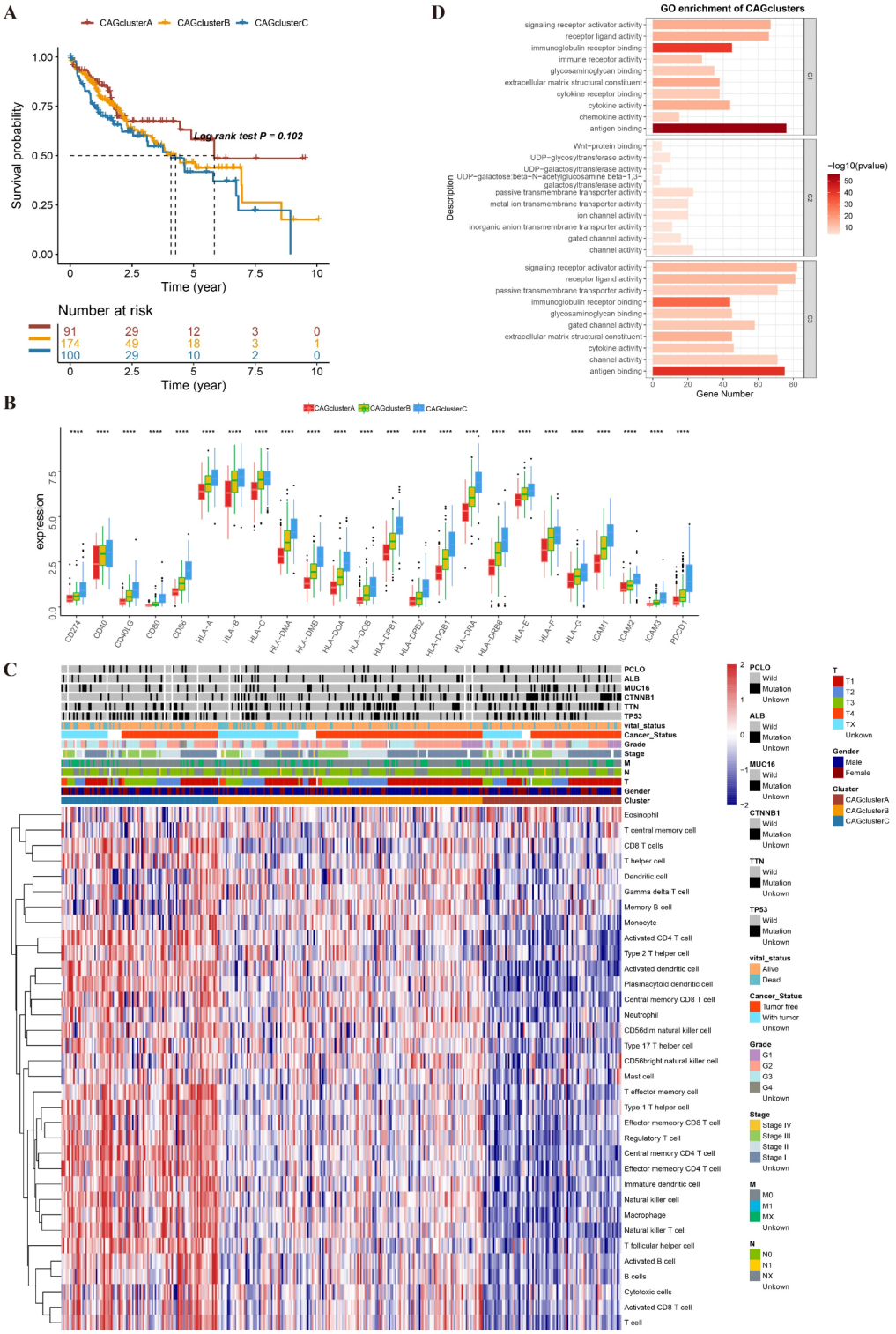

Fig. 4. Different characteristics of three coagulation-related patterns in the TCGA-LIHC cohort. (A) Kaplan-Meier curves with a log-rank test of three coagulation-related patterns in the TCGA-LIHC cohort. (B) Differential expression of costimulatory molecules, MHC molecules, and adhesion molecules in three coagulation-related patterns in TCGA-LIHC cohort. (C) Hierarchical clustering analysis of immune cell infiltration for HCC patients among three coagulation-related patterns in the TCGA-LIHC cohort. (D) Gene Ontology enrichment analysis in different coagulation-related patterns.

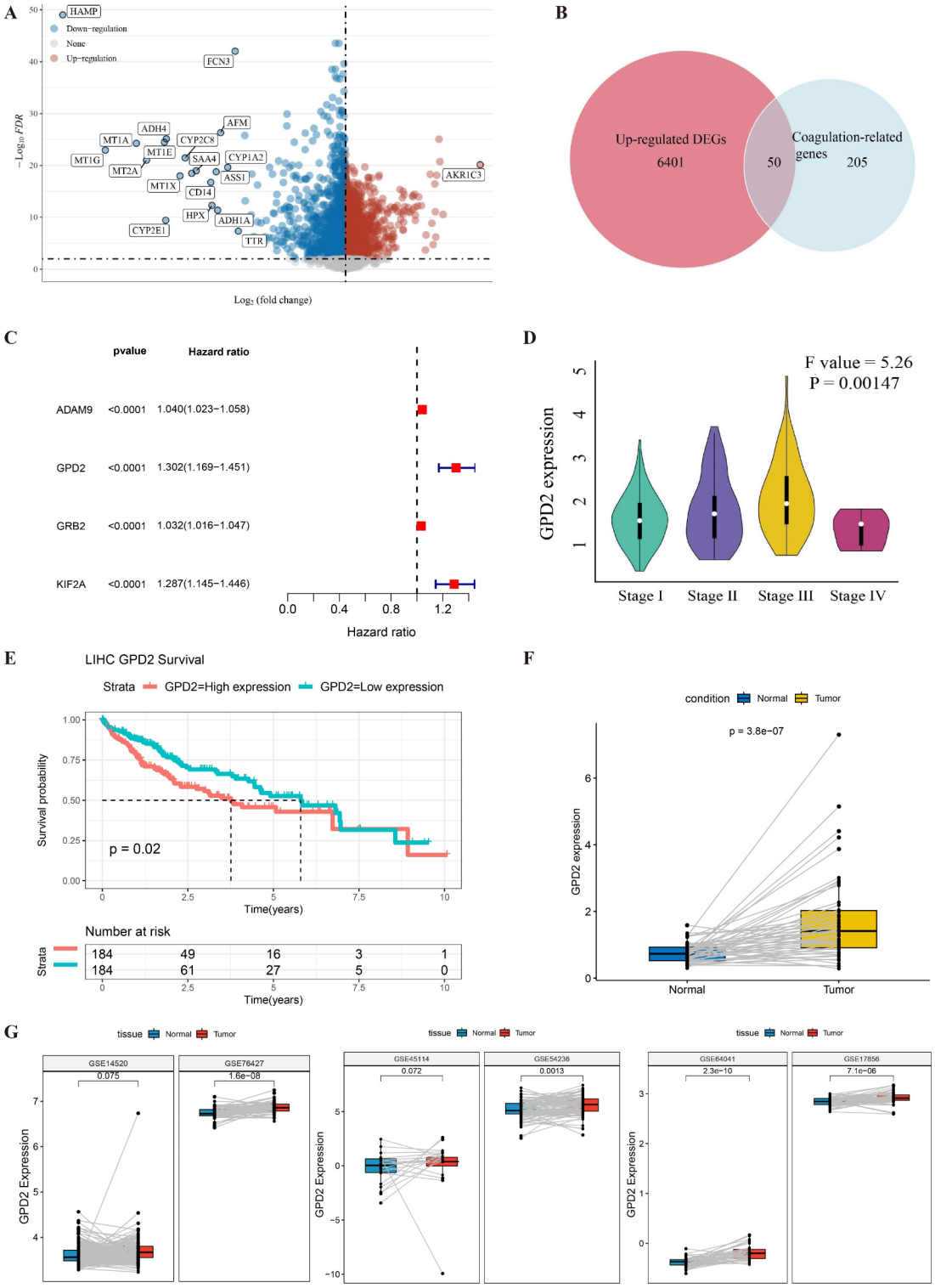

Fig. 5. Screening of target gene GPD2 and its differential expression in hepatocellular carcinoma. (A) Differentially expressed genes (DEGs) analysis in GSE76427. (B) Intersection analysis of coagulation-related gene set and up-regulated DEGs. (C) Univariate Cox regression analysis. (D) Differential expression of GPD2 in TCGA-LIHC in different clinical tumor stages. (E) Survival analysis of different GPD2 expression levels represented by Kaplan-Meier curve. (F) Differential expression of GPD2 in TCGA-LIHC cohort between tumor tissues and normal tissues. (G) Differential expression of GPD2 in multiple GEO datasets.

(ADAM9, GPD2, GRB2, and KIF2A) (Fig. 5C). GPD2 was chosen as the target gene for further analyses in HCC due to its most significant hazard ratio (HR) and limited literature in tumors. We found that GPD2 expression was discrepant in different tumor stages of HCC, and its expression was upregulated to a certain extent with the progression of the tumor stage (Fig. 5D). In addition, the HCC patients with low-GPD2 expression had better OS than those with high-GPD2 expression (Fig. 5E). Finally, differential expression analysis of GPD2 was performed in TCGA-LIHC and several GEO datasets. In the TCGA-LIHC dataset, GPD2 expression was significantly upregulated in HCC tumor tissues compared to adjacent tissues (Fig. 5F). In the GSE14520, GSE76427, GSE45114, GSE54236, GSE64041, and GSE17856 datasets, GPD2 levels were also upregulated to varying degrees in tumor tissue, similar to its expression pattern in TCGA-LIHC (Fig. 5G).

GPD2 was associated with immune microenvironment and immune evasion

Firstly, we conducted a correlation analysis between the GPD2 gene and HCC immune infiltration. We found that its expression was positively correlated with Th2 cells, T helper cells, Tfh cells, and macrophages, while negatively correlated with Th17 cells (Fig. 6A). Th2 cells mainly secrete IL-4, IL-5, IL-10, and IL-13, which are closely related to tumor progression and immune escape. We further analyzed the correlation between GPD2 expression and several vital immune-gene features, such as T cell-inflamed GEP, CAF, TAM M2, IFNG, CD8, CD274, TLS, T cell dysfunction, T cell exclusion, and MDSC. We found a strong positive correlation between GPD2 and immune-gene signatures such as MDSC and T cell exclusion in HCC (Fig. 6B). This indicates that the expression of GPD2 may promote immune suppression. In addition, the expression of inhibitory immune checkpoint genes predicts immune escape but can provide a reference for the selection of immunotherapy drugs. Therefore, we analyzed the correlation between the GPD2 gene and the expression of several inhibitory immune checkpoint genes. As demonstrated in Fig. 6C–F, GPD2 expression was significantly positively correlated with programmed death-1 (PD-1), programmed cell death ligand 1 (PD-L1), cytotoxic T lymphocyte-associated antigen-4 (CTLA-4), and CD47 molecule. This implies that in HCC, as the expression of GPD2 increases, the immune escape mediated by inhibitory immune checkpoints may be enhanced, but it may benefit from immunotherapy. The gene expression patterns related to T cell activation (CD3D, CD8A, CD28, LCK and S100A8), neutrophil activation (CXCR1, CXCR2, CXCL8, IL1R1, and IL1R2), and regulation of inflammatory response (MMP8, MMP9, TLR4 and TLR6) between the high-GPD2 and low-GPD2 groups of HCC were compared. These above key regulatory molecules and chemokines were highly expressed in the high-GPD2 group, compared to the low-GPD2 group (Fig. 7A–C). This may indicate a certain degree of activation of innate immune, adaptive immunity, and inflammatory response in the high-GPD2 group. Unfortunately, high-GPD2 expression was positively correlated with the tumor immune escape signature in HCC ($R = 0.49$, $P = 1.58e{-}23$) based on the TIP database (Fig. 7D). In addition, compared to the high-GPD2 group, the low-GPD2 group had higher cancer immune cycle scores in the release of cancer cell antigen, immune cell infiltration, and killing of cancer cells (Fig. 7E). The above results indicate that the expression of GPD2 may promote tumor immune escape and serve as a potential immunosuppressive target.

Biological process and function analysis of GPD2

In HCC, genes contained in relevant signaling pathways were collected and the correlation between GPD2 and biological signature was analyzed. We found that GPD2 expression was strongly positively correlated with multiple tumor-related signaling pathways, including angiogenesis ($R = 0.22$, $P = 2.57e{-}05$), inflammatory response ($R = 0.27$, $P = 9.9e{-}08$), tumor proliferation signature ($R = 0.47$, $P = 2.9e{-}22$), degradation of extracellular matrix (ECM) ($R = 0.29$, $P = 9.36e{-}09$), p53 pathway ($R = 0.35$, $P = 7.63e{-}12$), and PI3K-AKT-mTOR pathway ($R = 0.54$, $P = 2.43e{-}29$) (Fig. 8A–F). In the MEXPRESS database, we noticed that GPD2 expression was closely associated with different clinical factors, including adjacent hepatic tissue inflammatory response, histological type, tumor stage, sample type, and OS (Fig. 9A). In addition, there was a weak negative correlation between GPD2 mRNA expression and its DNA methylation levels (Fig. 9B). Sensitivity analyses of small molecule targeting and chemotherapy drugs were performed in the high-GPD2 and low-GPD2 groups. The results showed that the half-maximal inhibitory concentration (IC50) values of sorafenib and AKT inhibitor VIII were significantly lower in the high-GPD2 group compared to the low-GPD2 group (Fig. 9C, D). These outcomes suggest that the expression of GPD2 may affect the efficacy of chemotherapy and targeted therapy.

Verification of the roles of GPD2 in HCC cells

In this section, we performed qPCR to verify the expression of the GPD2 gene in HCC cell lines. We found that GPD2 was significantly upregulated in HepG2 and Huh7 cells compared to normal liver cells (Fig. 10A). IHC staining showed a significant increase in GPD2 expression in liver cancer tissues compared to adjacent normal tissues (Fig. 10B). We then transfected HepG2 and Huh7 cell lines with siRNA to successfully knock down the GPD2 mRNA expression (Fig. 10C). CCK-8 assay showed that GPD2 knockdown could significantly inhibit the proliferation of liver cancer cells (Fig. 10D). Furthermore, the colony formation assay was performed in HepG2 and Huh7 cells to further evaluate the proliferation of HCC cells. The results showed a significant decrease in the colony formation of GPD2 knockdown cell lines (Fig. 10E). To evaluate the migration and invasiveness of hepatocarcinoma, we performed the wound-healing and Transwell assays in HepG2 and Huh7 cells. The results showed that GPD2 gene knockdown could significantly inhibit the migration of HepG2 and Huh7 cells (Fig. 10F, G). The Matrigel invasion experiment also showed that GPD2 knockdown could significantly inhibit the invasion of HCC cells (Fig. 10H). Moreover, flow cytometry showed that GPD2 inhibition could obviously enhance the apoptosis rate of HepG2 and Huh7 cells (Fig. 10I).

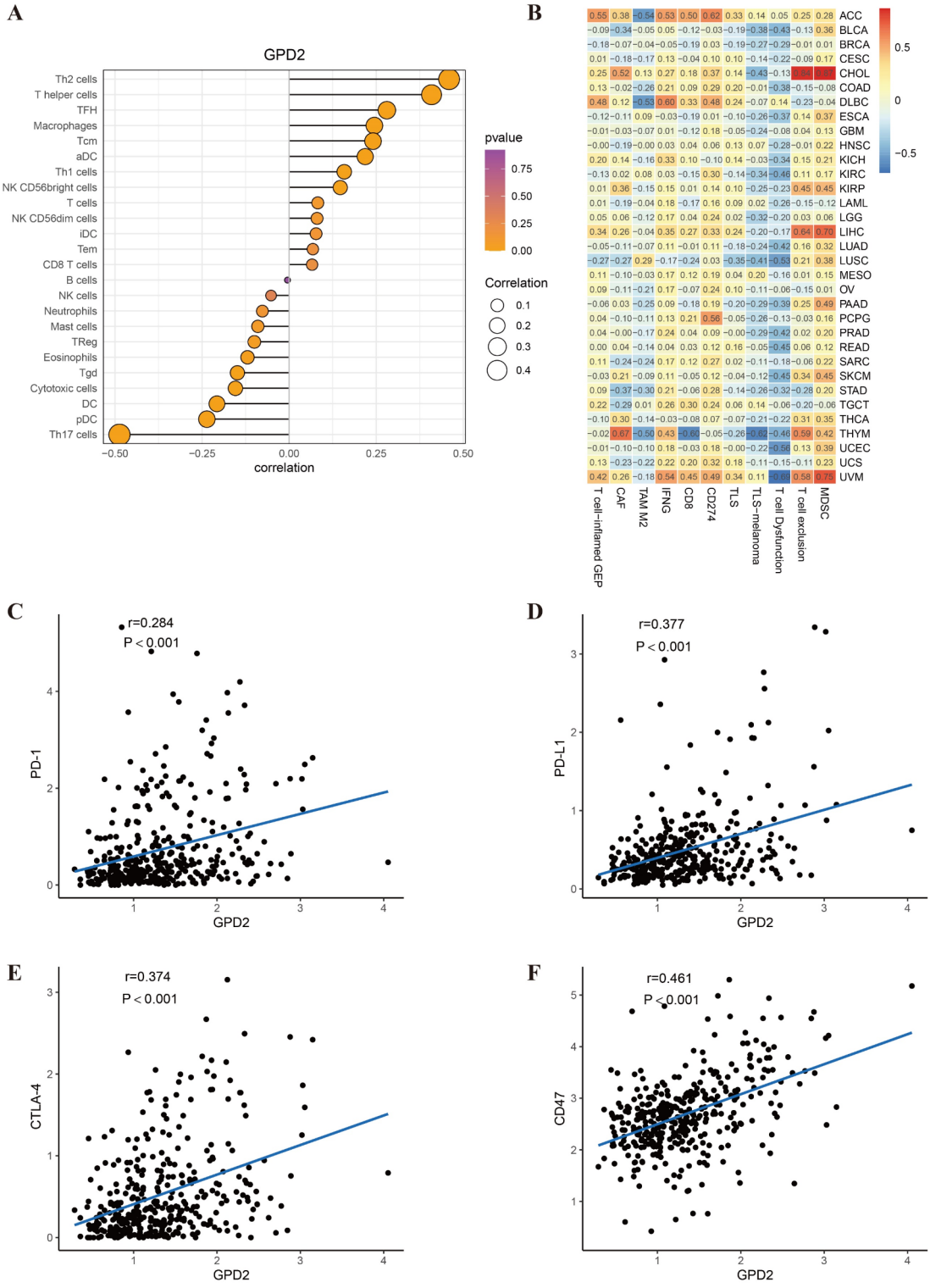

Fig. 6. Roles of GPD2 in the immune infiltration and immune checkpoint gene expression in hepatocellular carcinoma. (A) Correlation between GPD2 and immune cell infiltration in hepatocellular carcinoma. (B) Correlation of GPD2 and immune characteristic gene set of pan-cancer. (C-F) Correlation analysis between GPD2 and the expression of immune checkpoint genes, including PD-1 (C), PD-L1 (D), CTLA-4 (E) and CD47 (F).

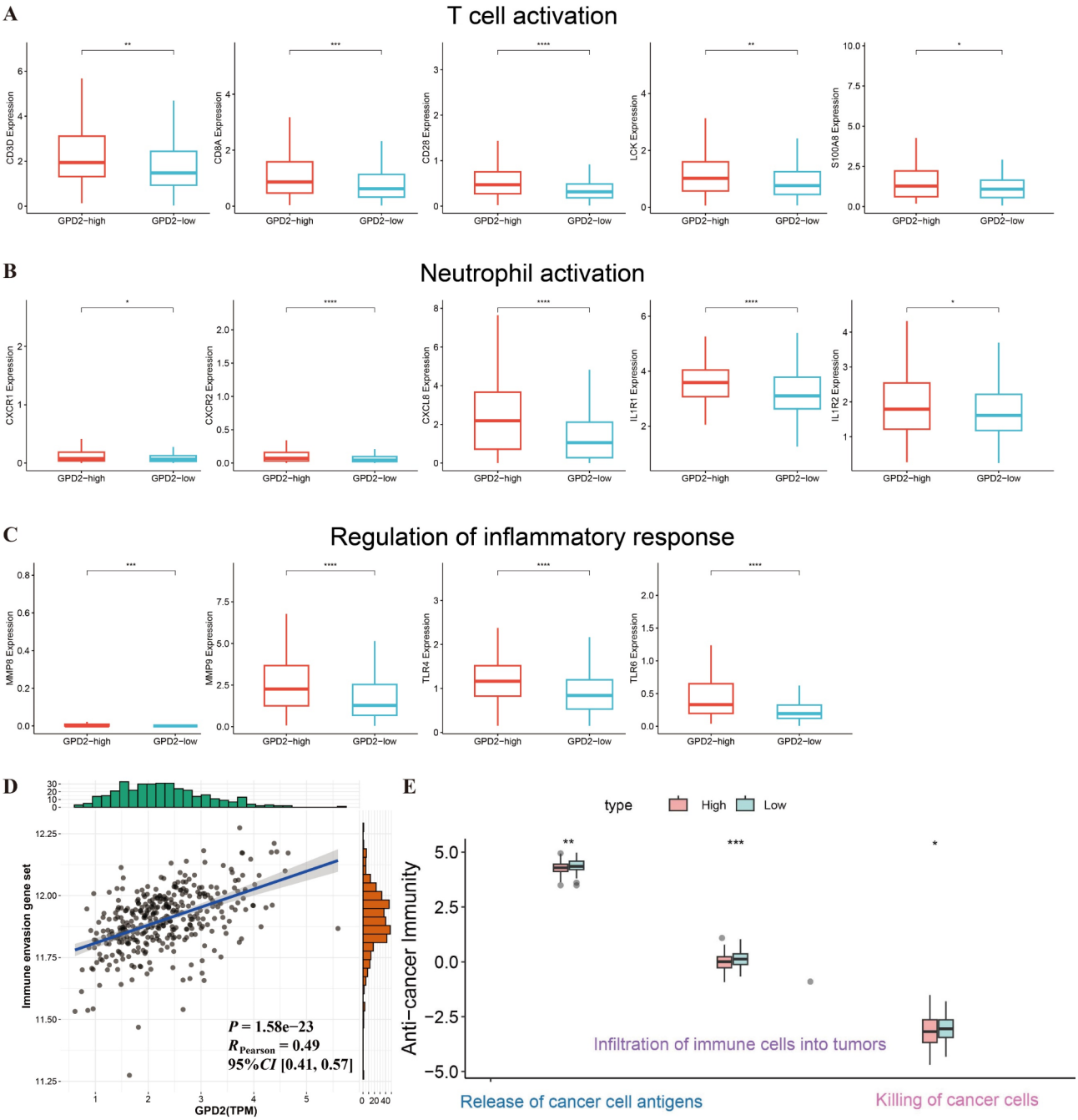

Fig. 7. Discrepancy in immunological pathways of immune infiltrating cells between different GPD2 expression levels. (A-C) Characteristic gene expression of T cell activation (A), neutrophil activation (B), and regulation of inflammatory response (C) between different GPD2 expression groups. (D) Correlation analysis between GPD2 expression and characteristic gene set of immune escape pathway. (E) Discrepancy in cancer-immunity cycle scores between different GPD2 expression groups.

Discussion

HCC poses a significant threat to human health, with its incidence and mortality rates rising steadily each year[20]. Although advancements in surgical techniques, chemotherapies, targeted therapies, immunotherapies, and the combination of targeted therapies with immunotherapies have improved prognostic outcomes for HCC patients, the overall results remain suboptimal. In recent years, evidence supporting the link between tumors and clotting disorders has been mounting. Hypercoagulability is common in tumor patients because tumor and surgery are the inevitable factors to induce thromboembolic events[21–23]. Patients with HCC often face a substantial risk of venous thromboembolism, with portal vein thrombosis being the most prevalent manifestation, affecting approximately 20–40% of cases[6,24]. Conversely, impaired coagulation function significantly elevates the risk

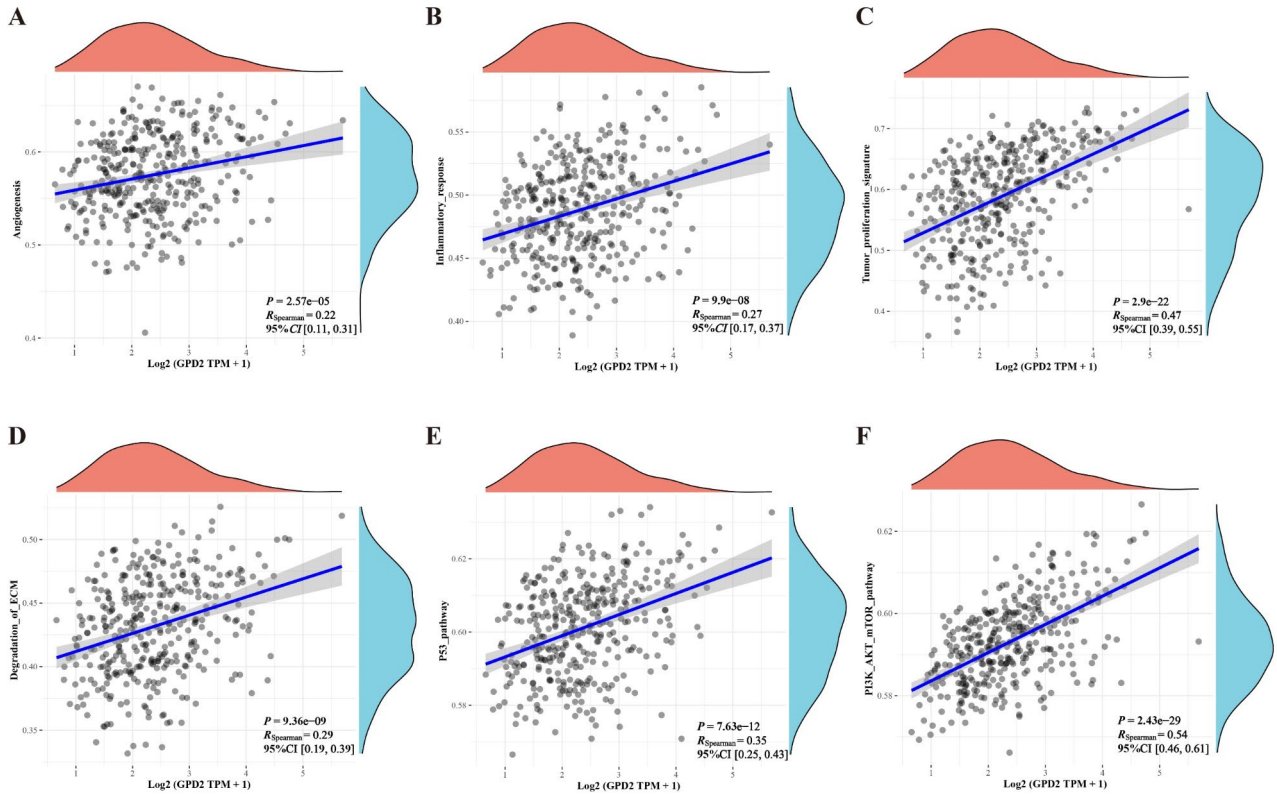

Fig. 8. Correlation analysis of GPD2 and tumor-related signaling pathways based on single-sample gene sets enrichment analysis. (A-F) Correlation analysis between GPD2 expression and various pathways including angiogenesis (A), inflammatory response (B), tumor proliferation (C), extracellular matrix degradation (D), p53 pathway (E), and PI3K-Akt-mTOR pathway (F).

associated with surgical interventions, creating a clinical dilemma for patients when choosing appropriate treatment strategies[25,26]. These findings highlight the critical role of coagulation in the pathophysiology of HCC. Investigating the interplay between coagulation pathways and HCC prognosis, immune infiltration, and TME, as well as identifying novel therapeutic targets linked to coagulation, may offer valuable insights into HCC treatment strategies. Therefore, this study aims to elucidate the influence of CAGs on tumor progress, prognosis, and the immune microenvironment in HCC.

In this study, unsupervised clustering algorithms were applied to classify the meta-LIHC dataset into three distinct CAGcluster patterns based on CAGs. These CAGclusters exhibited varying prognostic outcomes, immune cell infiltration, and MHC molecular expression. Subsequently, the same algorithms were performed in the validated TCGA-LIHC dataset to identify these distinct CAG patterns, and similar results regarding prognosis and immune infiltration were observed. Notably, CAGclusterC was characterized by a high level of immune cell infiltration, such as B cells, $CD4^+$ T cells, $CD8^+$ T cells, Tfh cells, Tregs, and MDSC, meaning that CAGclusterC may be more inclined to "hot tumor" properties. Among these infiltrating cells, activated $CD8^+$ T cells, often referred to as cytotoxic T lymphocytes, directly mediate anti-tumor immunity by recognizing and eliminating tumor cells in the TME. Furthermore, B cells participate in the presentation of tumor antigens to T cells and the release of cytokines to promote antitumor immunity, but they can also promote the formation of immune suppressor cells by releasing some immunosuppressive cytokines, thus inhibiting the anti-tumor response of effector T cells[27]. However, Tregs and MDSC are recognized as notorious immunosuppressive cells due to their ability to inhibit anti-tumor immune response by secreting immunosuppressive cytokines or expressing co-inhibitory molecules[28,29]. Unfortunately, more infiltrations of Tregs and MDSC in the CAGclusterC were found together, which may be an underlying reason for the unsatisfactory prognosis in these HCC patients. Briefly, although the patients in CAGclusterC had more abundant immune infiltration and immune response conditions, these infiltrated immune cells were doped with immunosuppressive factors. These findings reflect the complexity of the TME and suggest that therapeutic strategies targeting Tregs and MDSC should be developed for these patients.

To explore prognostic CAGs, we analyzed DEGs between HCC samples and adjacent normal samples and performed COX regression analysis for these differential genes. Ultimately, four risk genes associated with HCC prognosis were identified. Among these, GPD2 was selected for further investigation due to its most significant HR and limited research in the field of oncology. GPD2 is an encoded enzyme located on the human 2q24.1 chromosome, located on the inner-outer surfaces of the mitochondrial membrane[30]. As a key component of the mammalian respiratory chain and glycerol phosphate shuttle, it plays a pivotal role at the intersection of

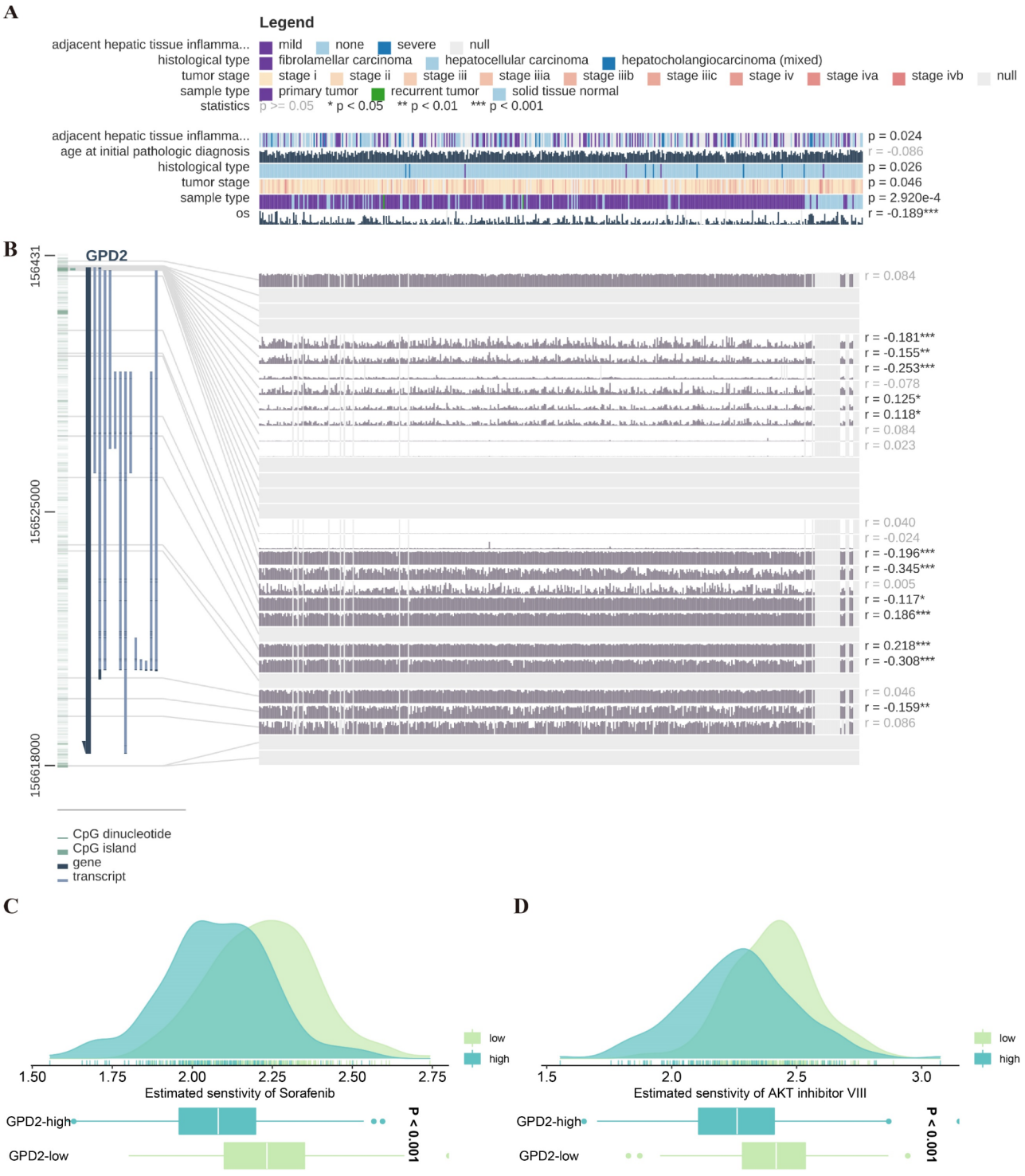

Fig. 9. Relevance between GPD2 and clinicopathological features, DNA methylation, and drug sensitivity in hepatocellular carcinoma. (A) Correlations between GPD2 expression and clinicopathological characteristics. (B) The correlation of GPD2 expression and DNA methylation level in the MEXPRESS database; $^{*}p < 0.05$, $^{**}p < 0.01$, and $^{***}p < 0.001$. (C-D) Discrepancy of drug sensitivity between different GPD2 expression groups.

glycolysis, oxidative phosphorylation, and fatty acid metabolism[31,32]. GPD2 can promote the production of reactive oxygen species that are commonly elevated in many tumor microenvironments and closely related to carcinogenesis[33,34]. Upregulating GPD2 expression in thyroid cancer has been shown to enhance oxidative phosphorylation, thereby promoting the growth of tumor cells[35]. In gliomas, GPD2 can facilitate tumor cell proliferation by increasing the rate of glycolysis[36]. Additionally, GPD2 knockdown has been demonstrated to

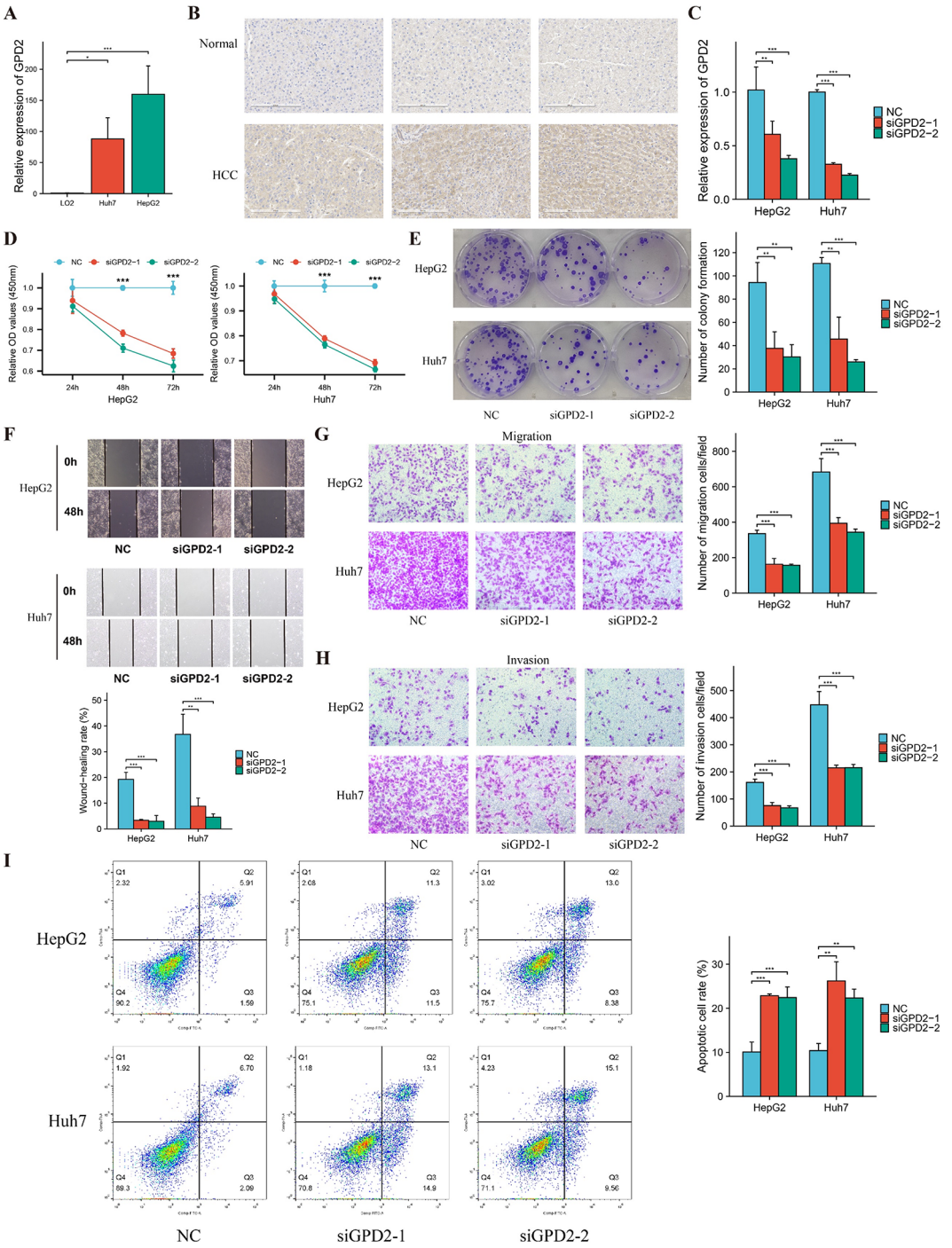

Fig. 10. Validation of the expression and roles of GPD2 in hepatocarcinoma in vitro. (A) Differential expression of GPD2 in HepG2 and Huh7 tumor cell lines and LO2 normal cell line. (B) Immunohistochemistry staining for GPD2 in adjacent non-tumor tissues and tumor tissues. (C) Inhibition of GPD2 expression in hepatocarcinoma using GPD2-targeted siRNA. (D) CCK-8 assay showed that the proliferation ability of HepG2 and Huh7 cells was significantly decreased after the inhibition of GPD2 expression. (E) Colony formation abilities of HepG2 and Huh7 cells were decreased after GPD2 knockdown. (F) Wound-healing assay showed that the migration distance of HepG2 and Huh7 cells was significantly reduced after the inhibition of GPD2 expression. (G) Transwell migration assay showed that inhibition of GPD2 expression could significantly reduce the migration ability of HepG2 and Huh7 cells. (H) Matrigel invasion assay showed that GPD2 knockdown could significantly reduce the invasion ability of HepG2 and Huh7 cells. (I) Apoptosis assay showed that GPD2 knockdown could significantly induce the death of HepG2 and Huh7 cells. $^{*}P<0.05$, $^{**}P<0.01$, and $^{***}P<0.001$.

reduce anchorage-independent cell proliferation in hepatocarcinoma[37]. GPD2 overexpression in prostate cancer cells has enhanced cellular wound-healing ability, indicating its regulatory roles in promoting tumor migration and metastasis[38]. Our study demonstrated that GPD2 was highly expressed in HCC and its expression was closely associated with advanced clinicopathological features and poor prognosis of HCC. Attenuating its expression in HCC cells could observably inhibit the proliferation, migration, and invasion, and promote the apoptosis of tumor cells. These findings imply that GPD2 is a biomarker of HCC progression and prognosis.

Moreover, the molecular mechanism by which GPD2 regulates HCC progression remains obscure. We noticed that GPD2 expression was closely related to multiple tumor-related signaling pathways, such as angiogenesis, tumor proliferation pathways, degradation of ECM, and PI3K-AKT-mTOR pathway. We hypothesize that GPD2 may participate in these signaling pathways, thus facilitating tumor progression and metastasis. Evidence showed that GPD2 knockdown resulted in the downregulation of the AKT/mTOR signaling pathway, thus inhibiting tumor growth[30]. This finding supports the regulatory roles of GPD2 in tumor progression by modulating key signaling pathways, while also highlighting its potential as a therapeutic target for HCC.

We further analyzed the GPD2 gene that was found to be associated with HCC progression and prognosis, to elucidate its potential roles in the tumor immune microenvironment. Th1 and Th2 cells, the two main subpopulations of T helper cells, are in a relatively balanced state by secreting cytokines that suppress each other's immune response. Once the transition from antitumor Th1 to protumor Th2 immunophenotype occurs, the Th1/Th2 balance will be broken, which is one of the decisive factors in tumorigenesis and progression[39]. We found that GPD2 expression had the most significant positive correlation with Th2 cell infiltration in TME, which may contribute to a disadvantaged antitumor immune response or even immune escape. In addition, GPD2 was positively correlated with the expression levels of multiple inhibitory immune checkpoints, such as PD-1, PD-L1, CTLA-4, and CD47. These immunosuppressive regulators are responsible for the immune escape in HCC[40]. For instance, CD47, known as the "Don't eat me" signal, prevents macrophage-mediated tumor cell phagocytosis, further promoting immune escape[41,42]. Evidence from the TIP database also confirmed the relationship between GPD2 and the immune escape of HCC. More importantly, we found a strong positive correlation between GPD2 expression and T cell exclusion in HCC. In the TME, effective antitumor immunity requires not only the generation of tumor-specific $CD8^+$ T cells but also physical contact of these T cells with tumor cells[43]. However, other components in the TME, such as stromal cells, can limit the antitumor immunity of T cells by excluding T cells in the vicinity of tumor cells, leading to the co-existence of T cells and tumor cells and the phenomenon of immune amnesty[43]. This also will bring great challenges to immunotherapy. Hence, targeting GPD2 may disrupt immune suppression and enhance the efficacy of immunotherapies. Overall, these findings pave the way for exploring GPD2 as a novel therapeutic target, particularly in combination with immunotherapy. Further research should aim to elucidate the mechanistic roles of GPD2 in regulating immune escape and reshaping the immune microenvironment of HCC in the future.

Despite the valuable insights provided by our study, several limitations should be acknowledged. First, these analyses are primarily based on bioinformatics data from public databases, which may suffer from inherent biases and lack of clinical validation. Second, while our study identifies GPD2 as a potential biomarker and therapeutic target, its regulatory details in immune escape and tumor progression in HCC require further in-depth experimental validation. Additionally, the efficacy of targeted GPD2 in HCC treatment remains to be evaluated through preclinical and clinical trials. Finally, the complex interactions between CAGs and the TME require more comprehensive studies to understand the underlying mechanisms. Future research should focus on the following areas to build upon our findings. First, prospective clinical studies are essential to validate the role of GPD2 as a prognostic biomarker in HCC and its association with immune escape. Preclinical models, including animal studies, should be employed to explore the therapeutic potential of GPD2 inhibitors and assess their effects on tumor growth, metastasis, and immune modulation. Additionally, investigating the precise molecular mechanisms through which GPD2 interacts with key signaling pathways, such as PI3K-AKT-mTOR, angiogenesis, and immune evasion pathways, will provide a deeper understanding of its oncogenic functions. Finally, expanding the scope of research to include other types of cancer could help determine whether GPD2 serves as a universal biomarker and therapeutic target in malignancies driven by similar mechanisms.

Conclusion

In conclusion, our study has comprehensively elucidated the coagulation-related characteristics in prognosis and immune microenvironment of HCC and identified a promising oncogenic gene GPD2. Further analyses have revealed that GPD2 is a potential biomarker for the progression, prognosis, and immune escape of HCC. Exploring targeted strategies based on coagulation-related characteristics and biomarkers may shed light on HCC treatment.

Data availability

The datasets generated and analysed during the current study are available from the corresponding author on reasonable request. The data that support the results of current study is available on public databases, including TCGA (https://gdc.cancer.gov/) and GEO (https://www.ncbi.nlm.nih.gov/geo/), in which the accession number s are as follows: GSE14520, GSE76427, GSE45114, GSE54236, GSE64041, and GSE17856.

Received: 27 September 2024; Accepted: 3 January 2025
Published online: 13 March 2025

References

1. Sung, H. et al. Global Cancer statistics 2020: GLOBOCAN estimates of incidence and mortality worldwide for 36 cancers in 185 countries. *CA Cancer J. Clin.* **71**, 209–249. https://doi.org/10.3322/caac.21660 (2021).
2. Llovet, J. M. et al. Hepatocellular carcinoma. *Nat. Rev. Dis. Prim.* **7**, 6. https://doi.org/10.1038/s41572-020-00240-3 (2021).
3. Pinter, M., Jain, R. K. & Duda, D. G. The current landscape of immune checkpoint blockade in hepatocellular carcinoma: a review. *JAMA Oncol.* **7**, 113–123. https://doi.org/10.1001/jamaoncol.2020.3381 (2021).
4. Huang, C. et al. A sodium alginate-based multifunctional nanoplatform for synergistic chemo-immunotherapy of hepatocellular carcinoma. *Adv. Mater. (Deerfield Beach Fla)* **2023**, e2301352. https://doi.org/10.1002/adma.202301352 (2023).
5. Khorana, A. A. et al. Cancer-associated venous thromboembolism. *Nat. Rev. Dis. Prim.* **8**, 253. https://doi.org/10.1038/s41572-022-00336-y (2022).
6. Connolly, G. C. et al. Incidence, risk factors and consequences of portal vein and systemic thromboses in hepatocellular carcinoma. *Thrombos Res.* **122**, 299–306. https://doi.org/10.1016/j.thromres.2007.10.009 (2008).
7. Dvorak, H. F. Tumors: wounds that do not heal-a historical perspective with a focus on the fundamental roles of increased vascular permeability and clotting. *Sem Thromb. Hemostas.* **45**, 576–592. https://doi.org/10.1055/s-0039-1687908 (2019).
8. Repetto, O. & De Re, V. Coagulation and fibrinolysis in gastric cancer. *Ann. N Y Acad. Sci.* **1404**, 27–48. https://doi.org/10.1111/nyas.13454 (2017).
9. Liu, J., Liu, B., Diao, G. & Zhang, Z. Tissue factor promotes HCC carcinogenesis by inhibiting BCL2-dependent autophagy. *Bull. Cancer* **109**, 795–804. https://doi.org/10.1016/j.bulcan.2022.04.007 (2022).
10. Schwarz, C. et al. Von Willebrand factor antigen predicts outcomes in patients after liver resection of hepatocellular carcinoma. *Gut Liver* **14**, 218–224. https://doi.org/10.5009/gnl17115 (2020).
11. Lok, A. S. et al. Des-gamma-carboxy prothrombin and alpha-fetoprotein as biomarkers for the early detection of hepatocellular carcinoma. *Gastroenterology* **138**, 493–502. https://doi.org/10.1053/j.gastro.2009.10.031 (2010).
12. Song, P. et al. Biomarkers: evaluation of screening for and early diagnosis of hepatocellular carcinoma in Japan and China. *Liver Cancer* **2**, 31–39. https://doi.org/10.1159/000346220 (2013).
13. Yin, G. et al. Integrated analysis to identify the prognostic and immunotherapeutic roles of coagulation-associated gene signature in clear cell renal cell carcinoma. *Front. Immunol.* **14**, 1107419. https://doi.org/10.3389/fimmu.2023.1107419 (2023).
14. Wang, B. et al. Construction and validation of a novel coagulation-related 7-gene prognostic signature for gastric cancer. *Front. Genet.* **13**, 957655. https://doi.org/10.3389/fgene.2022.957655 (2022).
15. Grøndahl-Hansen, J. et al. High levels of urokinase-type plasminogen activator and its inhibitor PAI-1 in cytosolic extracts of breast carcinomas are associated with poor prognosis. *Cancer Res.* **53**, 2513–2521 (1993).
16. Gautier, L., Cope, L., Bolstad, B. M. & Irizarry, R. A. affy–analysis of Affymetrix GeneChip data at the probe level. *Bioinform. (Oxf. Engl.)* **20**, 307–315. https://doi.org/10.1093/bioinformatics/btg405 (2004).
17. Turvey, S. E. & Broide, D. H. Innate immunity. *J. Allergy Clin. Immunol.* **125**, 24–32. https://doi.org/10.1016/j.jaci.2009.07.016 (2010).
18. Dempsey, P. W., Vaidya, S. A. & Cheng, G. The art of war: innate and adaptive immune responses. *Cell. Mol. Life Sci.* **60**, 2604–2621. https://doi.org/10.1007/s00018-003-3180-y (2003).
19. Guan, C. et al. ZNF774 is a potent suppressor of hepatocarcinogenesis through dampening the NOTCH2 signaling. *Oncogene* **39**, 1665–1680. https://doi.org/10.1038/s41388-019-1075-0 (2020).
20. Siegel, R., Ma, J., Zou, Z. & Jemal, A. Cancer statistics, 2014. *CA Cancer J. Clin.* **64**, 9–29. https://doi.org/10.3322/caac.21208 (2014).
21. Lauw, M. N., van Doormaal, F. F., Middeldorp, S. & Buller, H. R. Cancer and venous thrombosis: current comprehensions and future perspectives. *Semin. Thrombos. Hemostas.* **39**, 507–514. https://doi.org/10.1055/s-0033-1343891 (2013).
22. Chew, H. K., Wun, T., Harvey, D. J., Zhou, H. & White, R. H. Incidence of venous thromboembolism and the impact on survival in breast cancer patients. *J. Clin. Oncol.* **25**, 70–76. https://doi.org/10.1200/jco.2006.07.4393 (2007).
23. Alexander, M. et al. Thromboembolism in lung cancer—an area of urgent unmet need. *Lung Cancer (Amsterd. Netherl.)* **84**, 275–280. https://doi.org/10.1016/j.lungcan.2014.02.009 (2014).
24. Timp, J. F., Braekkan, S. K., Versteeg, H. H. & Cannegieter, S. C. Epidemiology of cancer-associated venous thrombosis. *Blood* **122**, 1712–1723. https://doi.org/10.1182/blood-2013-04-460121 (2013).
25. Hemostatic balance in. patients with liver cirrhosis: report of a consensus conference. *Digest. Liver Dis.* **48**, 455–467. https://doi.org/10.1016/j.dld.2016.02.008 (2016).
26. Ghadimi, K., Levy, J. H. & Welsby, I. J. Perioperative management of the bleeding patient. *Br. J. Anaesthes.* **117**, iii18–iii30. https://doi.org/10.1093/bja/aew358 (2016).
27. Ma, Q. Y. et al. Function of follicular helper T cell is impaired and correlates with survival time in non-small cell lung cancer. *Int. Immunopharmacol.* **41**, 1–7. https://doi.org/10.1016/j.intimp.2016.10.014 (2016).
28. Granito, A. et al. Hepatocellular carcinoma in viral and autoimmune liver diseases: role of CD4 + CD25 + Foxp3 + regulatory T cells in the immune microenvironment. *World J. Gastroenterol.* **27**, 2994–3009. https://doi.org/10.3748/wjg.v27.i22.2994 (2021).
29. Qi, Y. et al. Targeted modulation of myeloid-derived suppressor cells in the tumor microenvironment: implications for cancer therapy. *Biomed. Pharmacother.* **180**, 117590. https://doi.org/10.1016/j.biopha.2024.117590 (2024).
30. Oh, S. et al. Non-bioenergetic roles of mitochondrial GPD2 promote tumor progression. *Theranostics* **13**, 438–457. https://doi.org/10.7150/thno.75973 (2023).
31. Mráček, T., Drahota, Z. & Houštěk, J. The function and the role of the mitochondrial glycerol-3-phosphate dehydrogenase in mammalian tissues. *Biochim. Biophys. Acta* **1827**, 401–410. https://doi.org/10.1016/j.bbabio.2012.11.014 (2013).
32. Zhang, S., Liu, C. & Zhang, X. Mitochondrial damage mediated by miR-1 overexpression in cancer stem cells. *Mol. Therapy Nucleic Acids* **20**, 881. https://doi.org/10.1016/j.omtn.2020.05.017 (2020).
33. Schoenfeld, J. D. et al. O(2)(·-) and H(2)O(2)-Mediated disruption of fe metabolism causes the differential susceptibility of NSCLC and GBM cancer cells to pharmacological ascorbate. *Cancer Cell.* **32**, 268. https://doi.org/10.1016/j.ccell.2017.07.008 (2017).
34. Yang, R. et al. Tumor microenvironment responsive metal nanoparticles in cancer immunotherapy. *Front. Immunol.* **14**, 258. https://doi.org/10.3389/fimmu.2023.1237361 (2023).
35. Thakur, S. et al. Metformin targets mitochondrial glycerophosphate dehydrogenase to control rate of oxidative phosphorylation and growth of thyroid cancer in vitro and in vivo. *Clin. Cancer Res.* **24**, 4030–4043. https://doi.org/10.1158/1078-0432.Ccr-17-3167 (2018).
36. Lu, J. et al. Tumor-associated macrophage interleukin-β promotes glycerol-3-phosphate dehydrogenase activation, glycolysis and tumorigenesis in glioma cells. *Cancer Sci.* **111**, 1979–1990. https://doi.org/10.1111/cas.14408 (2020).
37. Mikeli, M. et al. Contribution of GPD2/mGPDH to an alternative respiratory chain of the mitochondrial energy metabolism and the stemness in CD133-positive HuH-7 cells. *Genes Cells* **25**, 139–148. https://doi.org/10.1111/gtc.12744 (2020).
38. Pecinová, A. et al. Role of mitochondrial glycerol-3-phosphate dehydrogenase in metabolic adaptations of prostate cancer. *Cells* **9**, 1764. https://doi.org/10.3390/cells9081764 (2020).
39. Shang, Q. et al. Polysaccharides regulate Th1/Th2 balance: a new strategy for tumor immunotherapy. *Biomed. Pharmacother.* **170**, 115976. https://doi.org/10.1016/j.biopha.2023.115976 (2024).
40. Li, Q., Han, J., Yang, Y. & Chen, Y. PD-1/PD-L1 checkpoint inhibitors in advanced hepatocellular carcinoma immunotherapy. *Front. Immunol.* **13**, 1070961. https://doi.org/10.3389/fimmu.2022.1070961 (2022).
41. Hayat, S. M. G. et al. CD47: role in the immune system and application to cancer therapy. *Cell. Oncol. (Dordrecht Netherlands)* **43**, 19–30. https://doi.org/10.1007/s13402-019-00469-5 (2020).

42. Li, W., Wang, F., Guo, R., Bian, Z. & Song, Y. Targeting macrophages in hematological malignancies: recent advances and future directions. *J. Hematol. Oncol.* **15**, 110. https://doi.org/10.1186/s13045-022-01328-x (2022).
43. Joyce, J. A. & Fearon, D. T. T cell exclusion, immune privilege, and the tumor microenvironment. *Sci. (N. Y. N. Y.)* **348**, 74–80. https://doi.org/10.1126/science.aaa6204 (2015).

Acknowledgements
We sincerely appreciate Dr. Chengjian Guan from Beijing Friendship Hospital, Capital Medical University for his help and support in the data analysis and research conception of this study.

Author contributions
D.L. conceived and designed the study. G.Q., K.L., and W.X. collected and analyzed the data. G.Q. conducted the experiment. G.Q. wrote the original manuscript. D.L. reviewed and edited the manuscript. All authors read and approved the final manuscript.

Competing interests
The authors declare no competing interests.

Ethical approval
was approved by the ethics committee of Beijing Friendship Hospital, Capital Medical University.

Additional information
Supplementary Information The online version contains supplementary material available at https://doi.org/10.1038/s41598-025-85491-4.

Correspondence and requests for materials should be addressed to D.L.

Reprints and permissions information is available at www.nature.com/reprints.

Publisher's note Springer Nature remains neutral with regard to jurisdictional claims in published maps and institutional affiliations.

Open Access This article is licensed under a Creative Commons Attribution-NonCommercial-NoDerivatives 4.0 International License, which permits any non-commercial use, sharing, distribution and reproduction in any medium or format, as long as you give appropriate credit to the original author(s) and the source, provide a link to the Creative Commons licence, and indicate if you modified the licensed material. You do not have permission under this licence to share adapted material derived from this article or parts of it. The images or other third party material in this article are included in the article's Creative Commons licence, unless indicated otherwise in a credit line to the material. If material is not included in the article's Creative Commons licence and your intended use is not permitted by statutory regulation or exceeds the permitted use, you will need to obtain permission directly from the copyright holder. To view a copy of this licence, visit http://creativecommons.org/licenses/by-nc-nd/4.0/.

© The Author(s) 2025